

## **ANALYTICAL AND NUMERICAL STUDIES OF NATURAL CONVECTION ALONG DOUBLY INFINITE VERTICAL PLATES IN STRATIFIED FLUIDS**

**Alan SHAPIRO\*, Evgeni FEDOROVICH, Jr.\***

\*School of Meteorology, University of Oklahoma, 120 David L. Boren Blvd, Norman, OK  
73072, USA

**Summary** Results are presented from a series of analytical and numerical studies of buoyantly driven flows along heated vertical surfaces immersed in stably stratified fluids. Flows of the studied type are broadly represented in engineering and geophysical applications. First, the classical problem of one-dimensional natural convection flow along a heated wall is revisited for the case of a stably stratified ambient fluid. The study then focuses on laminar natural convection in a viscous stably stratified fluid resulting from temporally periodic variations in the wall surface temperature. Finally, scaling relationships are proposed for the turbulent convection flow along a heated wall and verified based on results of direct numerical simulations.

### **1. INTRODUCTION**

Buoyantly (or convectively) driven flows along walls with thermally perturbed surfaces immersed in stably stratified fluids are of fundamental significance for a variety of engineering and geophysical applications of fluid mechanics ([1], [2]). Such flows – especially in their unsteady and turbulent forms – are notoriously difficult to analyze and describe quantitatively. In the present paper, we focus on particular cases of flows from the considered class aiming at providing new insights into their physics and formal description.

The case of unsteady laminar one-dimensional natural convection along an infinite vertical plate provides one of the few scenarios for the considered flow type where the Boussinesq equations of motion and thermodynamic energy may be solved analytically [2]. Analytical solutions for unsteady one-dimensional laminar natural convection along an infinite vertical plate were obtained in the 1950's and 1960's for a variety of surface forcings, though with a restriction to non-stratified environments. The extension of the one-dimensional convection framework to include ambient stratification is a relatively recent development ([3]-[7]).

Shapiro and Fedorovich [5] considered a laminar convection flow in a stratified fluid adjacent to a doubly infinite plate. Analytical solutions were obtained for a Prandtl number of unity for the cases of impulsive (step) change in plate perturbation temperature, sudden application of a plate heat flux, and for arbitrary temporal variations in plate perturbation temperature or plate heat flux. Vertical motion in a stably stratified fluid was associated with a simple negative feedback mechanism: rising warm fluid cooled relative to the environment, whereas subsiding cool fluid warmed relative to the environment. Because of this feedback, the flow in stably stratified fluid eventually approached a steady state, whereas the corresponding flow in a non-stratified fluid did not.

In a companion study, Shapiro and Fedorovich [6] used a combination of analytical and numerical techniques to explore the dependence of laminar convection along the plate on the Prandtl number ( $Pr$ ). The developing boundary layers were found to be thicker, more vigorous,

and more sensitive to the Pr value at smaller Pr numbers ( $<1$ ) than at larger Pr numbers ( $>1$ ). The gross temporal behavior of the flow after the onset of convection was of oscillatory-decay type for Pr near unity, and of non-oscillatory-decay type for large Pr numbers.

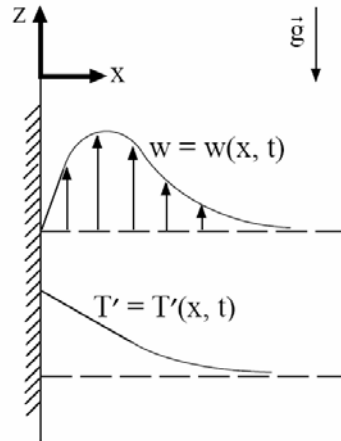


Fig. 1. Natural convection flow along a doubly infinite heated vertical plate

Another combined analytical and numerical study [7] focused on along-wall laminar natural convection flow resulting from temporally periodic variations in the surface temperature. Analytical temperature and velocity solutions were obtained for arbitrary values of ambient stratification, Pr number and forcing frequency. The solutions indicate that studied flow is composed of two waves that decay exponentially with distance from the surface: a fast long wave and a slow short wave. For forcing frequencies greater than the natural frequency of the corresponding inviscid system, these two waves propagate away from the surface. For forcing frequencies less than this natural frequency, the short wave propagates away from the surface while the long wave propagates toward the surface. This latter case provides an example of a flow for which the conventional radiation condition is not appropriate. The analytical results were complemented with three-dimensional numerical simulations of flows that start from rest being subjected to a periodic thermal forcing at the plate. The numerical results depicted the transient (start-up) stage of the flow and the approach to a periodic regime.

In the most recent study, we considered the same physical scenario as in [5] and [6], that is, natural convection along an infinite vertical wall in a stably stratified fluid, but for surface thermal forcings large enough that the flow becomes turbulent. Attention was restricted to the Prandtl number of unity and statistically stationary flow regimes. Scaling analyses in conjunction with direct numerical simulation (DNS) were employed to study this simplest class of turbulent natural convection flows. The derived scaling relationships were verified using the DNS data.

In the present paper, we summarize results from the above studies. The case of unsteady laminar convection flow with  $Pr=1$  and the extension of solutions to the case of arbitrary Pr are considered in section 2. Results from the study of forced periodic regime in the laminar convection flow along the wall are discussed in section 3. In section 4, we propose and verify scaling relationships for the turbulent convection along a heated wall in a stably stratified fluid.

## 2. UNSTEADY LAMINAR NATURAL CONVECTION

The governing Boussinesq equations for a three-dimensional flow with along a vertical wall in a right-hand Cartesian  $(x, y, z)$  frame attached to the wall (see Fig. 1) are the following:

$$\frac{\partial \mathbf{u}_i}{\partial t} + \mathbf{u}_j \frac{\partial \mathbf{u}_i}{\partial x_j} = -\frac{\partial p'}{\partial x_i} + \beta T' \delta_{i3} + \nu \frac{\partial^2 \mathbf{u}_i}{\partial x_j \partial x_j}, \quad (1)$$

$$\frac{\partial T'}{\partial t} + \mathbf{u}_j \frac{\partial T'}{\partial x_j} = -\gamma u_3 + \kappa \frac{\partial^2 T'}{\partial x_j \partial x_j}, \quad (2)$$

$$\frac{\partial \mathbf{u}_i}{\partial x_i} = 0, \quad (3)$$

where  $i=1, 2, 3$ ;  $j=1, 2, 3$ ;  $p' = (p - p_\infty) / \rho_r$  is the normalized deviation of pressure  $p$  from its hydrostatic value  $p_\infty(z)$ ,  $\rho_r$  is a constant reference density,  $\mathbf{u} = (u_1, u_2, u_3) \equiv (u, v, w)$  is the three-dimensional velocity vector with the components along the coordinate axes  $x \equiv x_1$  (wall-normal coordinate), and  $y \equiv x_2$ ,  $z \equiv x_3$  (along-wall coordinates),  $T' = T - T_\infty(z)$  is the perturbation temperature,  $T_\infty(z)$  is a linearly-varying ambient temperature,  $\gamma \equiv dT_\infty / dz + g / c_p$  is the stratification parameter;  $\nu$  is the kinematic viscosity,  $\kappa$  is the molecular thermal diffusivity;  $\beta = g / T_r$  is the buoyancy parameter ( $T_r$  is a constant reference temperature); and other symbols have their conventional meaning. The choice of boundary conditions for (1)-(3) depends on the flow setup. In the case of a doubly infinite wall (in real life, this would correspond to the smallness of boundary layer depth compared to flow dimensions on the  $z$ - $y$  plane), periodic boundary conditions in  $z$  and  $y$  directions could be set. The surface ( $x=0$ ) condition for temperature can be formulated either in terms of surface temperature or surface heat flux. In the first case, one may prescribe a constant surface temperature disturbance,  $T' = T'_0$  and assume no-slip surface boundary condition,  $w=0$  at  $x=0$ , and decay of flow disturbance at large  $x$ . The case of surface heat-flux condition allows a similar consideration, see [5].

By scaling the governing equations (1)-(3) with the following scales for length  $L_1$ , velocity  $V_1$ , temperature  $\theta_1$ , and time  $T_1$ :

$$L_1 \equiv \nu^{1/2} \gamma^{-1/4} \beta^{-1/4}, \quad V_1 \equiv T'_0 \gamma^{-1/2} \beta^{1/2}, \quad \theta_1 \equiv T'_0, \quad T_1 \equiv \gamma^{-1/2} \beta^{-1/2}, \quad (4)$$

and restricting our attention to the case of  $Pr = \nu / \kappa = 1$  we arrive at

$$\frac{\partial W_i}{\partial \tau} + Re_1 W_j \frac{\partial W_i}{\partial \xi_j} = -Re_1 \frac{\partial \Pi}{\partial \xi_i} + \theta \delta_{i3} + \frac{\partial^2 W_i}{\partial \xi_j \partial \xi_j}, \quad (5)$$

$$\frac{\partial \theta}{\partial \tau} + Re_1 W_j \frac{\partial \theta}{\partial \xi_j} = -W_3 + \frac{\partial^2 \theta}{\partial \xi_j \partial \xi_j}, \quad (6)$$

$$\frac{\partial W_i}{\partial \xi_i} = 0, \quad (7)$$

where  $Re_1 = L_1 V_1 / \nu = T'_0 \nu^{-1/2} \gamma^{-3/4} \beta^{1/4}$  is the Reynolds number based on l-scales (4), and  $W_i = u_i / V_1$ ,  $\theta = T' / \theta_1$ ,  $\xi_i = x_i / L_1$ ,  $\tau = t / T_1$  and  $\Pi = p' / V_1^2$  are the normalized velocity components, temperature perturbation, coordinates, and pressure disturbance, respectively. The plate boundary condition for the temperature perturbation becomes  $\theta_0 = T'_0 / \theta_1 = 1$ . For the case of parallel laminar flow, all terms with  $\xi_2$  and  $\xi_3$  derivatives vanish and the above system may be reduced to one-dimensional laminar flow equations

$$\frac{\partial W}{\partial \tau} = \theta + \frac{\partial^2 W}{\partial \xi^2}, \quad (8)$$

$$\frac{\partial \theta}{\partial \tau} = -W + \frac{\partial^2 \theta}{\partial \xi^2}, \quad (9)$$

considered in [5]. With  $Re_1 \gg 1$  the relative magnitude of nonlinear-convection and pressure-gradient terms in (5)-(7) increases and the along-wall flow may be expected to become unstable and then turbulent.

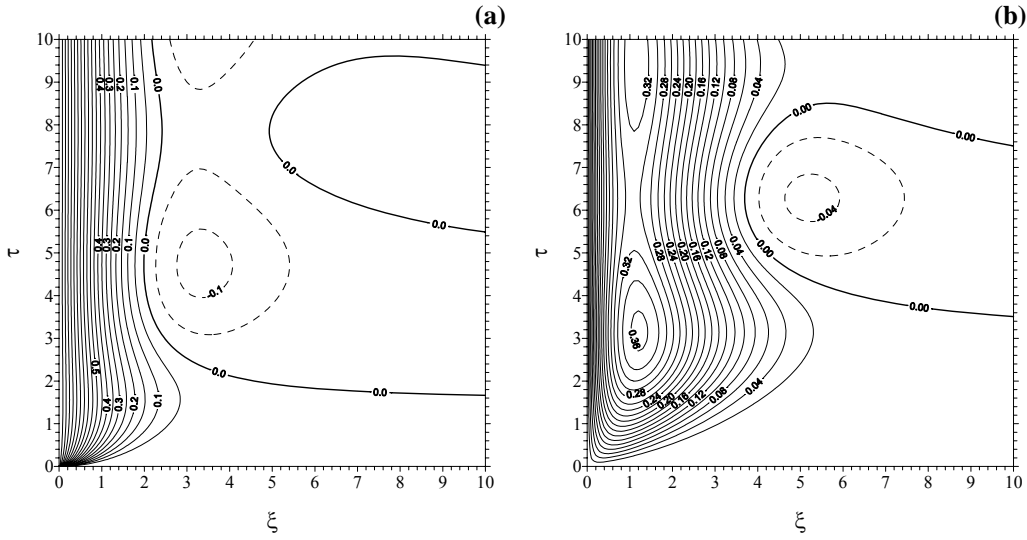


Fig. 2. Contours of (a)  $\theta(\xi, \tau)$  and (b)  $W(\xi, \tau)$  in the unsteady laminar convection flow

Next, we substitute  $W$  from (9) into (8) and obtain the fourth order equation for dimensionless temperature

$$\frac{\partial^2 \theta}{\partial \tau^2} + \frac{\partial^4 \theta}{\partial \xi^4} - 2 \frac{\partial^3 \theta}{\partial \xi^2 \partial \tau} + \theta = 0. \quad (10)$$

Multiplying (10) by  $e^{-st}$  and integrating (by parts, where possible) from  $\tau=0$  to  $\tau=\infty$  yields the ordinary differential equation

$$\frac{d^4 \hat{\theta}}{d\xi^4} - 2s \frac{d^2 \hat{\theta}}{d\xi^2} + (s^2 + 1) \hat{\theta} = 0. \quad (11)$$

where  $\hat{\theta} \equiv \int_0^{\infty} \theta e^{-s\tau} d\tau$  is the Laplace transform of  $\theta$ . A general solution of (11) for  $\hat{\theta}$  vanishing for  $\xi \rightarrow \infty$  is

$$\hat{\theta} = a \exp(-\xi\sqrt{s+i}) + b \exp(-\xi\sqrt{s-i}). \quad (12)$$

Evaluating coefficients  $a$  and  $b$  from the boundary conditions at the plate (which provides  $a=b=0.5 s^{-1}$ ), and taking the inverse transform of  $\hat{\theta}$ , we arrive at

$$\theta = \frac{1}{2} L^{-1} \left[ \frac{1}{s} \exp(-\xi\sqrt{s+i}) \right] + \frac{1}{2} L^{-1} \left[ \frac{1}{s} \exp(-\xi\sqrt{s-i}) \right]. \quad (13)$$

where  $L^{-1}$  denotes the inverse Laplace transform operator. The inverse transforms in (13) can be expressed as in [8]:

$$L^{-1} \left[ \frac{1}{s} \exp(-\xi\sqrt{s \pm i}) \right] = \frac{\xi}{2\sqrt{\pi}} \int_0^{\tau} \frac{1}{\tau'^{3/2}} \exp\left(-\mp i\tau' - \frac{\xi^2}{4\tau'}\right) d\tau'. \quad (14)$$

and so (13) becomes

$$\theta(\xi, \tau) = \frac{\xi}{2\sqrt{\pi}} \int_0^{\tau} \frac{\cos \tau'}{\tau'^{3/2}} \exp\left(-\frac{\xi^2}{4\tau'}\right) d\tau'. \quad (15)$$

The velocity field  $W$  is calculated from (9) with  $\theta$  supplied from (15). After integration by parts and rearrangement of terms, we obtain

$$W(\xi, \tau) = \frac{\xi}{2\sqrt{\pi}} \int_0^{\tau} \frac{\sin \tau'}{\tau'^{3/2}} \exp\left(-\frac{\xi^2}{4\tau'}\right) d\tau'. \quad (16)$$

Although it is not obvious, careful analysis of (15) shows that it provides the desired temperature value at the plate surface:  $\lim_{\xi \rightarrow 0} \theta(\xi, \tau) = 1$ . Differentiation of (15) with respect to  $\xi$  yields

$$-\frac{d\theta}{d\xi}(0, \tau) = \frac{\cos \tau}{\sqrt{\tau\pi}} + \frac{1}{\sqrt{2}}. \quad (17)$$

Thus, the plate heat flux is infinite at  $\tau=0$  and undergoes a decaying oscillation as it approaches  $1/\sqrt{2}$  in the limit  $\tau \rightarrow \infty$ . Since the non-dimensional period  $2\pi$  corresponds to a dimensional period of  $2\pi(\beta\gamma)^{-1/2}$ , stronger stratifications, or larger buoyancy parameter values, are associated with higher oscillation frequencies. Contour plots of  $\theta(\xi, \tau)$  and  $W(\xi, \tau)$  are presented in Fig. 2. These plots show the boundary-layer character of the solutions and the oscillatory approach to steady-state conditions.

Solutions for the considered flow case without ambient stratification (we will refer to those as the classical solutions) have the following form [9]:

$$\theta(\xi, \tau) = \operatorname{erfc}\left(\frac{\xi}{2\sqrt{\tau}}\right) = \frac{\xi}{2\sqrt{\pi}} \int_0^{\tau} \frac{1}{\tau'^{3/2}} \exp\left(-\frac{\xi^2}{4\tau'}\right) d\tau', \quad (18)$$

$$W(\xi, \tau) = \xi\sqrt{\tau} \cdot \operatorname{ierfc}\left(\frac{\xi}{2\sqrt{\tau}}\right) = -\frac{\xi^3}{4\sqrt{\pi}} \int_0^{\tau} \frac{1}{\tau'^{3/2}} \exp\left(-\frac{\xi^2}{4\tau'}\right) d\tau' + \frac{\xi\sqrt{\tau}}{\sqrt{\pi}} \exp\left(-\frac{\xi^2}{4\tau}\right), \quad (19)$$

where  $\operatorname{erfc}(x) \equiv \frac{2}{\sqrt{\pi}} \int_x^{\infty} \exp(-x'^2) dx'$  and  $\operatorname{ierfc}(x) \equiv \int_x^{\infty} \operatorname{erfc}(x') dx'$ . In order to facilitate the comparison, we non-dimensionalized the classical (non-stratified flow) solutions in the same manner as our new solutions.

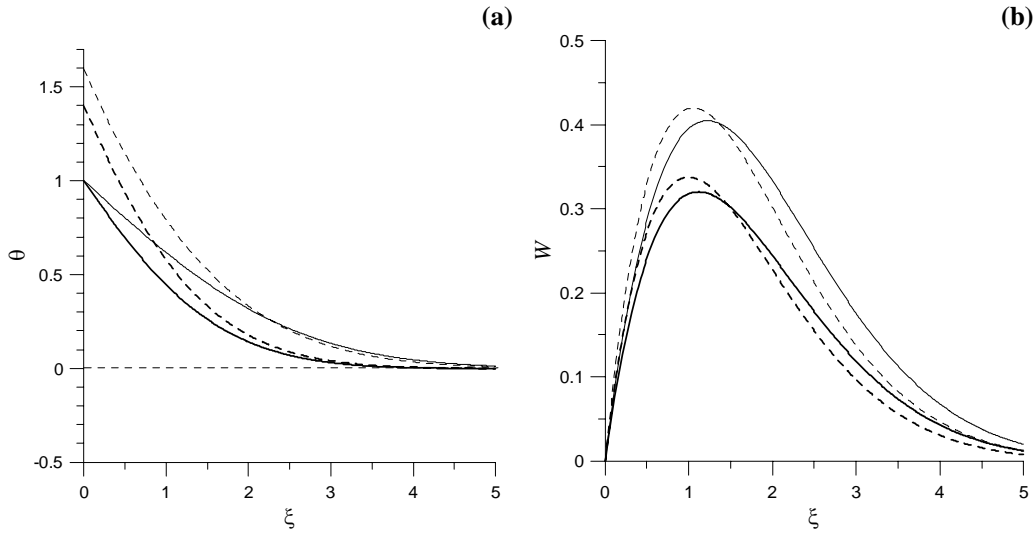


Fig. 3. Cross-sections of (a)  $\theta(\xi, \tau)$  and (b)  $W(\xi, \tau)$  at dimensionless time  $\tau = 2$ . Solid lines present classical solution and heavy solid lines present new solution for the case of an impulsive (step) change in plate perturbation temperature. Dashed lines present counterparts of classical and new solutions for the case of suddenly applied plate heat flux

New and classical solutions for the horizontal distributions of  $\theta(\xi, \tau)$  and  $W(\xi, \tau)$  at  $\tau = 2$  are compared in Fig. 3. It is clearly seen that the classical model predicts larger temperature perturbations and larger velocities than predicted by the new model that accounts for negative feedback mechanism associated with stratification. Also shown in Fig. 3 are the new and classical solutions for the flow case with the heat-flux boundary conditions at the wall from [5].

The steady-state solution for dimensionless temperature  $\theta_s(\xi)$  is obtained from (10) with time derivatives neglected. In this case, (10) reduces to a linear fourth-order ordinary differential equation, whose solution is given by

$$\theta_s(\xi) = \cos(\xi/\sqrt{2}) \exp(-\xi/\sqrt{2}), \quad (20)$$

The steady-state velocity  $W_s(\xi)$  is readily obtained from the steady version of (9):

$$W_s(\xi) = \sin(\xi/\sqrt{2}) \exp(-\xi/\sqrt{2}), \quad (21)$$

These solutions have a boundary-layer character in contrast to the non-stratified flow (classical) solutions, in which it is an inexorable conductively driven spread of the thermal disturbance outward from the plate, see [5].

Shapiro and Fedorovich [6] demonstrated how the analytical framework described above may be extended to the fluids of arbitrary Prandtl number, when equation (9) acquires the following form:

$$\frac{\partial \theta}{\partial \tau} = -W + \frac{1}{\text{Pr}} \frac{\partial^2 \theta}{\partial \xi^2}. \quad (9a)$$

Analytical solutions of (8) and (9a) with boundary conditions of either the surface-temperature or the surface-flux type may be obtained in the form of a perturbation expansion for Prandtl numbers near unity.

With  $\varepsilon$  defined as the deviation of the Prandtl number from unity,  $\varepsilon = \text{Pr} - 1$ , (9a) becomes

$$(1 + \varepsilon) \frac{\partial \theta}{\partial \tau} = -(1 + \varepsilon)W + \frac{\partial^2 \theta}{\partial \xi^2}. \quad (9b)$$

Multiplying (8) and (9b) by  $e^{-s\tau}$ , integrating them from  $\tau=0$  to  $\tau=\infty$ , and eliminating  $\hat{W} \equiv \int_0^\infty W e^{-s\tau} d\tau$  in favor of  $\hat{\theta} \equiv \int_0^\infty \theta e^{-s\tau} d\tau$ , we obtain:

$$\frac{d^4 \hat{\theta}}{d\xi^4} - s(2 + \varepsilon) \frac{d^2 \hat{\theta}}{d\xi^2} + (1 + \varepsilon)(s^2 + 1) \hat{\theta} = 0. \quad (22)$$

It can be readily shown that  $\hat{W}$  satisfies an equation of the same form as (22). With attention restricted to Pr near unity,  $\varepsilon$  is a small parameter, and solution of (22) for  $\hat{\theta}$ , as well as solution of analog of (22) for  $\hat{W}$ , may be sought in the form of regular perturbation expansions:

$$\hat{\theta} = \hat{\theta}_0 + \varepsilon \hat{\theta}_1 + \varepsilon^2 \hat{\theta}_2 + \dots = \sum_{n=0}^{\infty} \varepsilon^n \hat{\theta}_n, \quad (23)$$

$$\hat{W} = \hat{W}_0 + \varepsilon \hat{W}_1 + \varepsilon^2 \hat{W}_2 + \dots = \sum_{n=0}^{\infty} \varepsilon^n \hat{W}_n. \quad (24)$$

In [6], the zeroth-, first-, and second-order terms in the expansions were obtained for an impulsive change in plate temperature, while the zeroth- and first-order terms were obtained for a sudden application of a plate heat flux. It was shown that ensuing differential equations for  $\hat{\theta}_n$  and  $\hat{W}_n$  are independent of  $\varepsilon$ , so that after computing these Laplace transforms once, they can be applied in (23)-(24) to obtain the solutions for  $\hat{\theta}$  and  $\hat{W}$  for any Pr near unity. The

solutions for the original variables,  $\theta(\xi, \tau)$  and  $W(\xi, \tau)$ , follow by taking the inverse Laplace transform,  $L^{-1}$ , of  $\hat{\theta}$  and  $\hat{W}$ , and using the linearity of the  $L^{-1}$  operator:

$$\theta = \sum_{n=0}^{\infty} \varepsilon^n \theta_n, \quad W = \sum_{n=0}^{\infty} \varepsilon^n W_n, \quad (25)$$

where  $\theta_n \equiv L^{-1}(\hat{\theta}_n)$  and  $W_n \equiv L^{-1}(\hat{W}_n)$ .

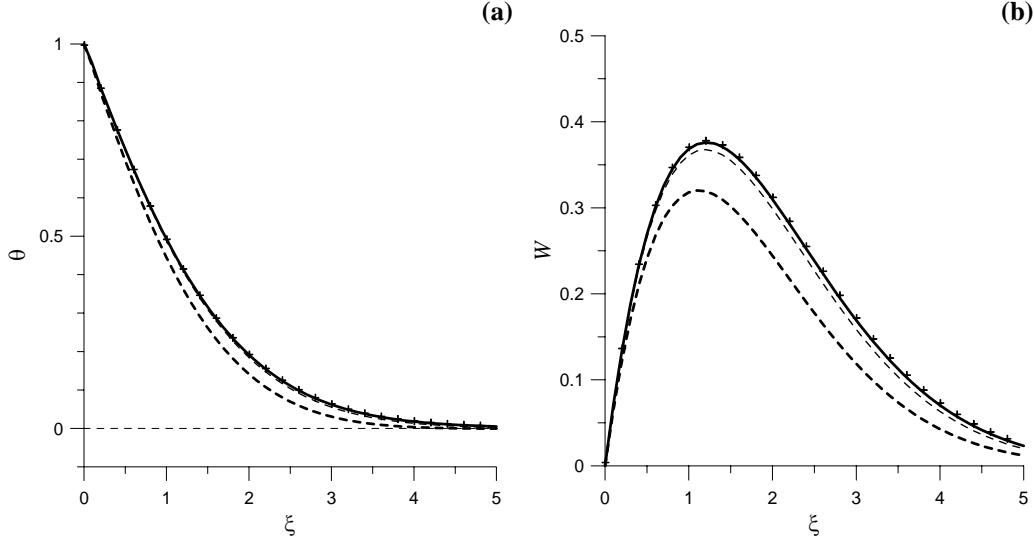


Fig. 4. Dimensionless temperature (a) and velocity (b) distributions at  $\tau = 2$  for the case of  $Pr=0.71$ . Numerical results are presented by plus symbols. Zeroth analytical approximations  $\theta_0$  and  $W_0$  (which correspond to the exact solution for  $Pr=1$ ) are shown by bold dashed lines. First analytical approximations  $\theta_0+\varepsilon\theta_1$  and  $W_0+\varepsilon W_1$  are shown by thin dashed lines, and second analytical approximations  $\theta_0+\varepsilon\theta_1+\varepsilon^2\theta_2$  and  $W_0+\varepsilon W_1+\varepsilon^2 W_2$  are shown by solid bold lines

The analytical solutions considered above are valid for  $Pr$  near unity. The exact forms of these solutions are presented in [6]. To explore the limits of validity of these analytical solutions and to extend the investigation to a wider range of  $Pr$  numbers, we additionally employed numerical simulations. The numerical procedures adopted in [6] were based on methods described in [10] applied in the direct numerical simulation (DNS) mode. The governing equations (1)-(3) were discretized on a staggered Cartesian grid in a rectangular domain stretched along the plate-normal  $x$  direction. The equations for the prognostic flow variables  $u$ ,  $v$ ,  $w$ , and  $T'$  were integrated over time using the leapfrog scheme with an Asselin time filter. The spatial derivatives were approximated with second-order finite-difference expressions. The Poisson equation for pressure was solved at each time step with a Fast Fourier Transform technique over the  $y$ - $z$  planes (vertical planes parallel to the plate), and a tri-diagonal factorization method in the plate-normal direction. No-slip and impermeability conditions were applied on the velocity components at the plate. Values of pressure gradient at the plate were calculated from the equation for the  $x$  component of momentum with imposed impermeability condition. At the opposite (large  $x$ ) end of the computational domain, the normal gradients of all prognostic

variables were set to zero. Periodic boundary conditions were imposed for all computed variables on the four x-y and x-z computational boundaries of the domain. The output velocity and temperature perturbation values were averaged over the y-z planes. However, as long as the flow remained laminar (which was the case for results reported in this section), variations of these quantities in the y-z planes were negligible. To facilitate comparisons with the analytical results, the output variables were non-dimensionalized as in (5)-(7).

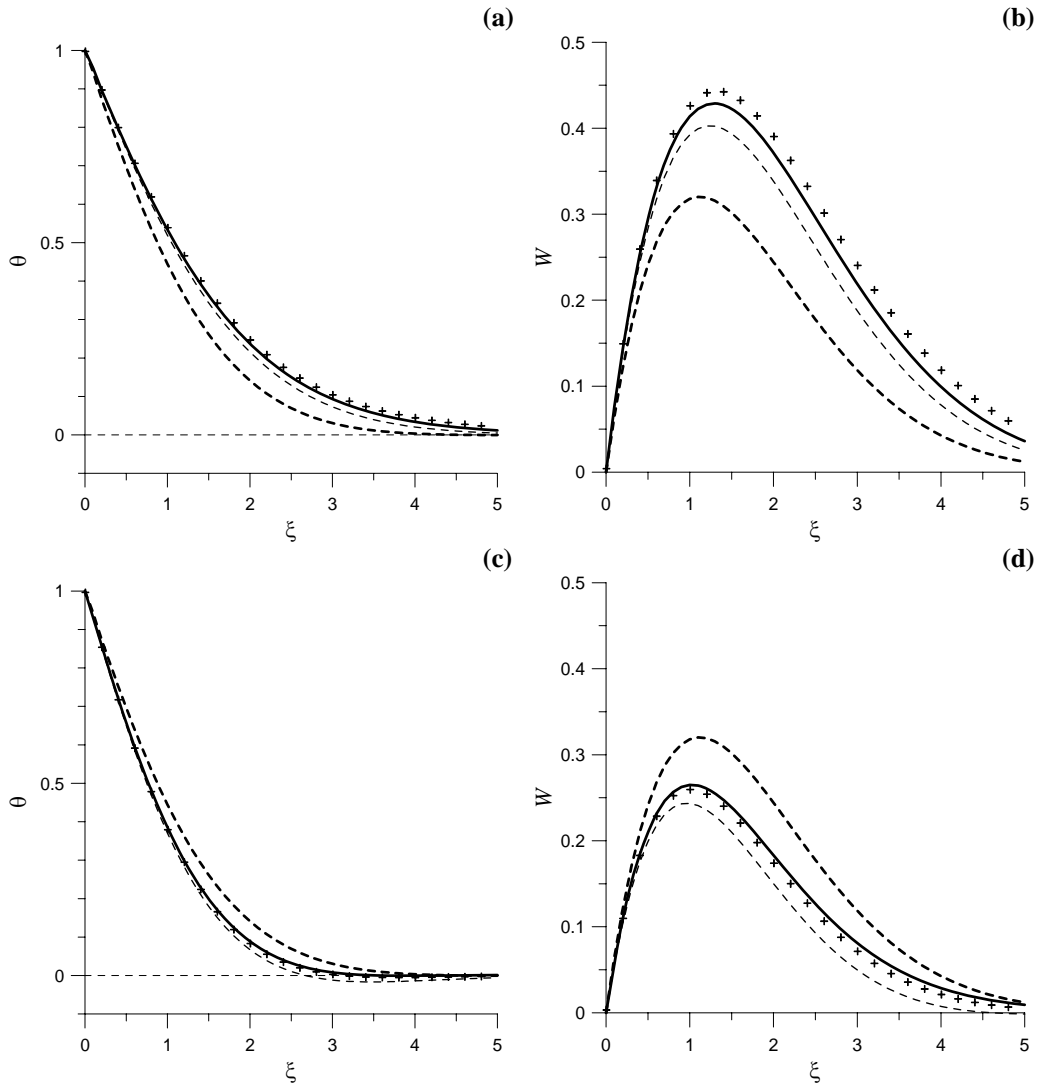


Fig. 5. As in Fig. 4, but for the cases of  $Pr=0.5$ , (a) and (b), and  $Pr=1.5$ , (c) and (d)

Cross-sections of the second-order approximate solutions at  $\tau = 2$  for the case of impulsive (step) change in plate perturbation temperature are presented in Fig. 4. Also shown in this figure are the first-order approximate solutions, the zeroth-order approximate solutions, and the

numerical solution. The differences between the second-order approximate solution and the numerical solution are nearly imperceptible throughout the cross-section. In the region of the peak vertical velocity, the first-order approximate solution falls a few percent short of the numerical solution, while the zeroth-order approximate solution falls nearly 20% short of the numerical solution.

Next we consider cross-sections of the analytical and numerical solutions at  $\tau = 2$  for the cases of  $Pr=0.5$  and  $Pr=1.5$ , see Fig. 6. Even though the  $Pr$  numbers for these cases are no longer very close to unity, the second-order approximate solution still follows the numerical solution rather closely. The presented cross-sections point to the increase in peak boundary-layer velocity and boundary layer thickness as the Prandtl number decreases. In general, the boundary layers developing along the wall in the investigated flow cases were found to be thicker, more vigorous and more sensitive to the  $Pr$  number at smaller  $Pr$  ( $<1$ ) than at larger  $Pr$  ( $>1$ ). The relative magnitudes of the sequence of zeroth-, first and second-order approximate solutions for  $\theta$  and  $W$  indicate the in-phase contributions of the zeroth-, first and second-order functions for  $Pr < 1$ , and the out-of-phase contribution of the first-order function with respect to the zeroth- and second-order functions for  $Pr > 1$ , see [6] for a more detailed interpretation.

In this manner, the accuracy of the analytical descriptions was explored in [6] for Prandtl numbers ranging between 0.5 and 1.5, including  $Pr=0.71$ , the value for dry air at a temperature of 30 °C and atmospheric pressure. The second-order approximate solution for the case of the impulsive change in plate temperature yielded a remarkably accurate flow description for  $Pr$  numbers in this range.

We also outlined in [6] a qualitative theory of flow behavior for arbitrary Prandtl number for the case of an impulsive change in plate temperature. The analysis considered the Fourier sine-transformed equations of motion, and examined the temporal behavior of each mode in wavenumber space as a function of  $Pr$ . The analysis showed that the gross behavior of flows with  $Pr$  numbers near unity is of oscillatory-decay type, while the gross behavior of flows with large  $Pr$  numbers is of non-oscillatory-decay type.

### 3. NATURAL CONVECTION FORCED BY TEMPORALLY-PERIODIC SURFACE TEMPERATURE VARIATIONS

In [7], we considered application of the one-dimensional laminar flow equations (8) and (9a) to study the natural convection flow induced in the stably stratified fluid adjacent to the vertical wall by periodic perturbations of the wall-surface temperature.

The corresponding inviscid system [dimensional version of (8) and (9a) with  $v=\kappa=0$ ] admits traveling wave solutions of the form  $w \propto \sin(kx - \sqrt{\beta\gamma}\tau)$  and  $T' \propto \cos(kx - \sqrt{\beta\gamma}\tau)$ , and *en masse* temporal oscillations of the form  $w \propto \sin(\sqrt{\beta\gamma}\tau)$  and  $T' \propto \cos(\sqrt{\beta\gamma}\tau)$ . These inviscid solutions have a frequency equal to the Brunt-Väisälä (buoyancy) frequency  $\sqrt{\beta\gamma}$ . The non-dimensional value of this frequency is unity.

The imposed perturbation temperature at the surface of the plate is a temporal oscillation with circular frequency  $\omega$  and an amplitude of unity,  $\theta(0, \tau) = \cos\omega\tau$ . This fixed amplitude is a consequence of the non-dimensionalization, and does not represent a loss of generality. Since the thermal forcing originates at the plate, and the medium is viscous, the disturbance is considered to vanish far from the plate, except for the case of resonance (imposed frequency equal to the natural frequency of the inviscid system,  $\omega=1$ ), where an extension of the disturbance to infinity is found to be unavoidable.

Solutions of (8) and (9a) were sought in [7] in the form of simple harmonic oscillations:

$$\theta = \Re[A(\xi) \exp(-i\omega\tau)], \quad W = \Re[B(\xi) \exp(-i\omega\tau)] \quad (26)$$

where  $A$  and  $B$  are complex-valued functions, and, without loss of generality,  $\omega$  may be considered to be positive.

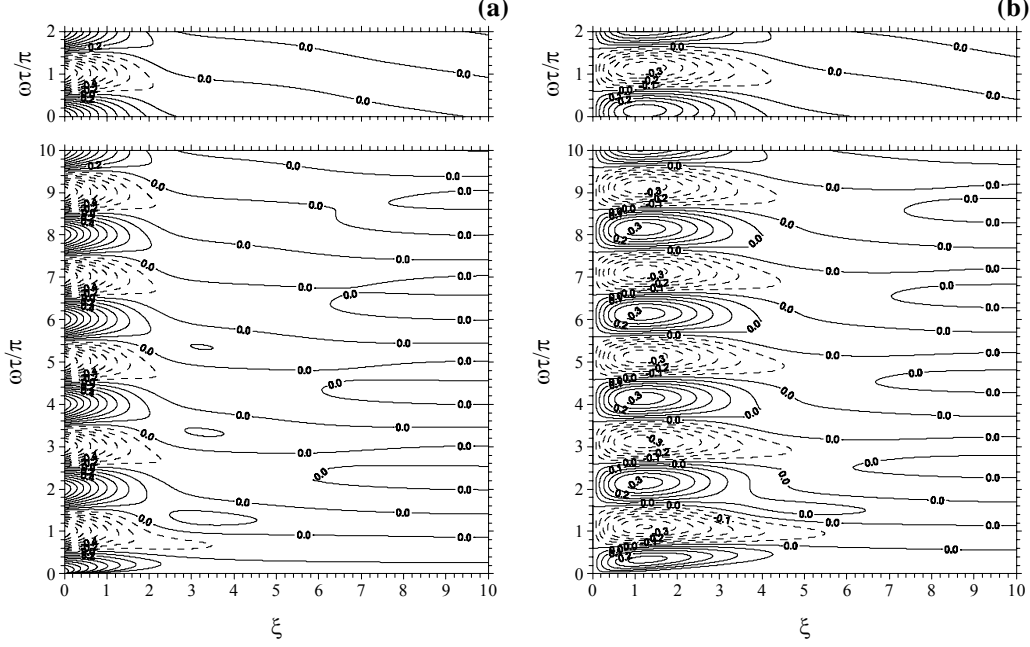


Fig. 6. Fields of  $\theta$  (a) and  $W$  (b) for  $Pr=1$  and  $\omega=0.5$  for the first five oscillation periods. Corresponding analytical solutions for one period of oscillation are presented at the top

Application of (26) in (8) and (9a) provides

$$-i\omega A = -B + \frac{1}{Pr} \frac{d^2 A}{d\xi^2}, \quad -i\omega B = A + \frac{d^2 B}{d\xi^2}, \quad (27)$$

whose solution is given by

$$\theta = \frac{1}{2}(1 + F_\theta) \exp(-k_+ \xi) \cos(k_+ \xi - \omega\tau) + \frac{1}{2}(1 - F_\theta) \exp(-k_- \xi) \cos(Sk_- \xi - \omega\tau), \quad (28)$$

$$W = F_W \exp(-k_+ \xi) \sin(k_+ \xi - \omega\tau) - F_W \exp(-k_- \xi) \sin(Sk_- \xi - \omega\tau), \quad (29)$$

where

$$F_\theta \equiv \frac{\omega(Pr-1)}{\sqrt{4Pr + \omega^2(Pr-1)^2}}, \quad F_W \equiv \frac{1}{\sqrt{4Pr + \omega^2(Pr-1)^2}},$$

$$k_+ \equiv \frac{1}{2} \sqrt{\omega(Pr+1) + \sqrt{4Pr + \omega^2(Pr-1)^2}}, \quad k_- \equiv \frac{1}{2} \sqrt{\omega(Pr+1) - \sqrt{4Pr + \omega^2(Pr-1)^2}},$$

and  $S$  is the sign function of  $\omega - 1$ :

$$S = \text{sgn}(\omega - 1) = \begin{cases} 1, & \omega > 1 \\ -1, & \omega < 1 \end{cases}.$$

The special case  $\omega = 1$  is considered separately below.

For  $\omega > 1$  ( $S = 1$ ,  $Sk_\xi > 0$ ), the solution is composed of two waves that propagate away from the plate and decay exponentially with distance from the plate. Since the phases of these waves are  $k_+ \xi - \omega \tau$  and  $Sk_- \xi - \omega \tau$ , we see that  $k_+$  and  $k_-$  can be interpreted as wavenumbers. Since  $k_+ > k_- > 0$ , the  $k_-$  wave has a larger wavelength ( $2\pi/k_-$ ), greater phase speed ( $\omega/k_-$ ), and larger e-folding penetration distance ( $1/k_-$ ) than the  $k_+$  wave.

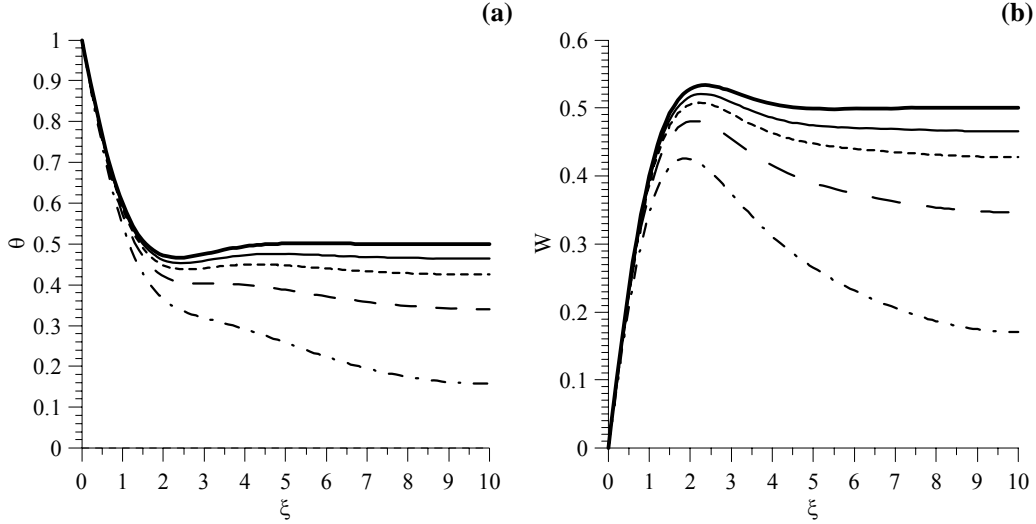


Fig. 7. Numerical solutions for  $\theta$  (left) and  $W$  (right) as functions of  $\xi$  at different  $2\pi$  intervals of time for  $Pr=1$  and  $\omega=1$ . Each  $W$  curve is a quarter-period ahead of the corresponding  $\theta$  curve. The  $\theta$  curves refer to  $\tau/\pi=8$  (dashed and dotted line),  $\tau/\pi=18$  (long-dash line),  $\tau/\pi=28$  (short-dash line), and  $\tau/\pi=38$  (solid line). Bold lines show the analytical solutions

For  $\omega < 1$  ( $S = -1$ ,  $Sk_\xi < 0$ ), the solution is again composed of a  $k_+$  wave and a  $k_-$  wave, each of which decays exponentially with distance from the plate, with the  $k_-$  wave having a greater wavelength, greater phase speed and greater penetration distance than the  $k_+$  wave. However, in this case, while the  $k_+$  wave still propagates away from the plate, the  $k_-$  wave propagates toward the plate. It can be shown that for both  $\omega < 1$  and  $\omega > 1$ , the  $k_+$  and  $k_-$  waves are each associated with positive group velocities, that is, energy propagating away from the plate.

The case of  $\omega = 1$  may be interpreted as a case of resonance (forcing frequency equal to the buoyancy frequency – the natural frequency of the inviscid system). A solution that vanishes at infinity is not possible in this case. However, one may require that the disturbance is bounded at infinity. The solution for the case  $\omega = 1$  is then found to be

$$\theta = \frac{\cos \tau}{1 + \text{Pr}} + \frac{\text{Pr}}{1 + \text{Pr}} \exp(-F_{\text{Pr}} \xi) \cos(F_{\text{Pr}} \xi - \tau), \quad W = \frac{\sin \tau}{1 + \text{Pr}} + \frac{1}{1 + \text{Pr}} \exp(-F_{\text{Pr}} \xi) \sin(F_{\text{Pr}} \xi - \tau), \quad (30)$$

where  $F_{\text{Pr}} \equiv \sqrt{(\text{Pr}+1)/2}$ . Thus, the resonance solution is comprised of an outward-propagating spatially-decaying wave and an *en masse* inviscid-like temporal oscillation.

A numerical procedure analogous to the one described in section 2 was applied in [7] to describe flows starting from rest that are suddenly subjected to a plate perturbation temperature. These numerical investigations were aimed at capturing the transient (start-up) stage of the flow and proving that the analytical solutions considered above provide the appropriate description of a later-stage periodic flow regime.

Figure 6 depicts numerical and analytical  $\theta$  and  $W$  solutions for  $\text{Pr}=1$  and  $\omega=0.5$ , a case where the forcing frequency is less than the natural frequency of the ambient fluid. In the region of the main disturbance, near the plate, the numerical solution approaches the analytical one within just a few oscillation periods. Far from the plate, the disturbance becomes weak and the negative slopes of the zero contours in the analytical solutions for  $\theta$  and  $W$  indicate an inward-propagating wave. Such negative slopes begin to emerge in the numerical solution at the later times in the figure.

Evolution of temperature and velocity profiles with time in the case of  $\text{Pr}=1$  and  $\omega=1$  (resonance case) is depicted in Fig. 7. Here, the numerical solution approaches the analytical solution at large  $\xi$  relatively slowly. The periodic regime is characterized by *en masse* oscillations of the entire fluid, with the exception of the boundary layer in the immediate vicinity of the plate whose structure is dominated by the no-slip condition.

#### 4. SCALING RELATIONSHIPS FOR TURBULENT NATURAL CONVECTION

With increasing surface buoyancy forcing, which corresponds to larger  $\text{Re}_1$  values in (5)-(7), the natural convection flow along the wall undergoes a transition to the turbulent regime. In this section, we will present a preliminary analysis of the scaling relationships in this regime.

Consider the dimensional governing equations (1)-(3) written in terms of buoyancy  $b \equiv -g[\rho - \rho_\infty(z)]/\rho_r \approx g[T - T_\infty(z)]/T_r = \beta T'$  (with  $\rho_\infty$  denoting the ambient density) and the Brunt-Väisälä (or buoyancy) frequency in the ambient stably stratified fluid  $N = \sqrt{\gamma\beta}$ . After applying in these equations the Reynolds decomposition of flow fields [ $\varphi = \bar{\varphi}(x) + \varphi'(t, x, y, z)$ , where  $\varphi$  is a generic flow variable,  $\bar{\varphi}(x)$  its average value that depends on the distance from the wall only, and  $\varphi'(t, x, y, z)$  is the turbulent perturbation of  $\varphi$ ], averaging the equations spatially (over  $y$ - $z$  planes) and temporally (over  $t$ ), using the properties of Reynolds averaging [11] with respect to velocity and buoyancy perturbations and to the  $y$  and  $z$  components of the perturbation pressure gradient, and finally applying the surface conditions of impermeability ( $u=0$  at  $x=0$ ) and no slip ( $v=w=0$  at  $x=0$ ), we obtain

$$b + \nu \frac{\partial^2 w}{\partial x^2} - \frac{\partial \overline{w'u'}}{\partial x} = 0, \quad (31)$$

$$-wN^2 + \kappa \frac{\partial^2 b}{\partial x^2} - \frac{\partial \overline{b'u'}}{\partial x} = 0, \quad (32)$$

$$-\frac{\partial \overline{p'}}{\partial x} - \frac{\partial \overline{u'u'}}{\partial x} = 0. \quad (33)$$

where (33) immediately integrates to the relationship  $\overline{p'} = -\overline{u'u'}$  (assuming that  $\overline{u'u'}$  vanishes both at  $x=0$  and  $x=\infty$ ). In (31) and (32),  $b$  now denotes mean buoyancy and  $w$  denotes the mean flow velocity component along the wall (with overbars omitted), while  $\overline{w'u'}$  and  $\overline{b'u'}$  represent  $x$  components of turbulent kinematic fluxes of mean momentum and buoyancy, respectively. In the remainder of this section, we will restrict our attention to a Prandtl number of unity ( $\text{Pr} = \nu/\kappa = 1$ ).

Equations (31) and (32) can be scaled with generic scales  $L$  (for distance),  $V$  (for velocity), and  $B$  (for buoyancy):

$$b_n + \frac{\nu V}{L^2 B} \frac{\partial^2 w_n}{\partial x_n^2} - \frac{V^2}{LB} \frac{\partial \tau_n}{\partial x_n} = 0, \quad (34)$$

$$-w_n + \frac{\nu B}{L^2 N^2 V} \frac{\partial^2 b_n}{\partial x_n^2} - \frac{B}{LN^2} \frac{\partial F_n}{\partial x_n} = 0, \quad (35)$$

where the normalized ( $n$ ) flow variables are defined as  $x_n = x/L$ ,  $w_n = w/V$ ,  $b_n = b/B$ ,  $\tau_n = \overline{w'u'}/V^2$ , and  $F_n = \overline{w'b'}/(VB)$ .

Below we propose scaling relationships between the generic scales and the basic parameters of the flow which are molecular diffusivity  $\nu$ , ambient Brunt-Väisälä frequency  $N$ , and surface forcing expressed in terms of surface buoyancy flux  $F_0$ . The proposed relationships are based on the following hypotheses regarding changes of flow structure with distance away from the wall:

- A. In the immediate vicinity of the wall, which we will call the interior flow region, or *i*-region, the flow is controlled entirely by the energy production rate at the surface (which in our problem is equal to the surface buoyancy flux) and molecular viscosity/diffusivity. We consider the characteristic flow length scale in this region to be much smaller than the length scale associated with the ambient stratification,  $g/N^2$ . Accordingly, the base-state advection term  $wN^2$  in (32) should be negligibly small, and the flow in this region should not be subject to the effects of ambient stratification.
- B. In contrast, at large distances from the surface, which we will call the exterior flow region, or *e*-region, the flow is essentially turbulent and the effects of molecular viscosity/diffusivity may be omitted from consideration. Flow structure in this region is determined exclusively by the surface energy production rate and ambient stratification.

Following the A hypothesis, we combine  $F_0$  and  $\nu$  to obtain the buoyancy-flux-based set of *i*-scales for distance, velocity, and buoyancy,

$$L_i = \nu^{3/4} F_0^{-1/4}, \quad V_i = \nu^{1/4} F_0^{1/4}, \quad B_i = \nu^{-1/4} F_0^{3/4}, \quad (36)$$

It can be noted that the length scale  $L_i$  weakly decreases with increasing surface forcing  $F_0$ .

According to the B hypothesis, sufficiently far from the wall, in the e-region, the flow structure is controlled by  $F_0$  and  $N$ . Combining these parameters, one obtains the e-scales for the length, velocity, and buoyancy, respectively,

$$L_e = F_0^{1/2} N^{-3/2}, \quad V_e = F_0^{1/2} N^{-1/2}, \quad B_e = F_0^{1/2} N^{1/2}. \quad (37)$$

All scales in the e-region are proportional to the root of  $F_0$ . In particular, the length scale  $L_e$  increases with increasing  $F_0$ , unlike the behavior of the length scale in the i-region. The e-scales (37) provide the following e-scaled equations of momentum and buoyancy balance

$$b_e + \left( \frac{F_0}{\nu N^2} \right)^{-1} \frac{\partial^2 w_e}{\partial x_e^2} - \frac{\partial \tau_e}{\partial x_e} = 0, \quad (38)$$

$$-w_e + \left( \frac{F_0}{\nu N^2} \right)^{-1} \frac{\partial^2 b_e}{\partial x_e^2} - \frac{\partial F_e}{\partial x_e} = 0, \quad (39)$$

with boundary conditions:

$$w_{e0} = 0, \quad (db_e/dx_e)|_0 = -F_0/(\nu N^2), \quad w_{e\infty} = 0, \quad b_{e\infty} = 0. \quad (40)$$

where  $x_e = x/L_e$ ,  $w_e = w/V_e$ ,  $b_e = b/B_e$ ,  $\tau_e = \overline{w'u'}/V_e^2$ , and  $F_e = \overline{w'b'}/(V_e B_e)$ .

One may consider two separate Reynolds numbers based on the i and e scales defined in (36) and (37):

$$Re_i = \frac{L_i V_i}{\nu} = 1, \quad Re_e = \frac{L_e V_e}{\nu} = \frac{F_0}{\nu N^2} \equiv Re. \quad (41)$$

The scales in the i and e regions are related through  $Re = F_0/(\nu N^2)$  as

$$L_e/L_i = Re^{3/4}, \quad V_e/V_i = Re^{1/4}, \quad B_e/B_i = Re^{-1/4}, \quad (42)$$

so in our further analyses we will be using  $Re = Re_e$ , which uniquely determines the structure of the e-scaled governing equations (38)-(39) as a master Reynolds number.

Using (37), we evaluate the Richardson number  $Ri = L_e B_e / V_e^2$  (the square of the inverse Froude number,  $Fr$ ), commonly used in analyses of atmospheric stratified turbulent flows [12], as  $Ri = 1$  (which also gives  $Fr=1$ ). Furthermore, again using (37),  $Re$  may be related to the Rayleigh number  $Ra = B_e L_e^3 / \nu^2$  as  $Re = Ra^{1/2}$ . Note that in our problem with  $Pr=1$  the Rayleigh number is equivalent to the Grashof number ( $Gr$ ).

The expression  $L_i = \nu^{3/4} F_0^{-1/4}$  in (36) indicates that this length scale may be treated as a characteristic turbulence length scale in the i-region, that is, an analog of the Kolmogorov microscale [11]. Because  $L_i$  is related to the surface stress scale as  $L_i = \nu / \sqrt{\tau_0}$ , it may also be considered as an analog of the viscous length scale, which serves as the depth scale of the viscous sublayer in the immediate vicinity of the wall ([11], p. 270).

We may also consider a length scale that does not include the surface buoyancy forcing. Such a scale is identified as  $L_m = \nu^{1/2} N^{-1/2}$ . In view of (36) and (37), this length scale can be

expressed as  $L_m = V_e L_i / V_i$ , so one may interpret it as an analog of the Taylor microscale extensively discussed in [11] and [13]. It is easy to see that  $L_m$  is related to  $L_i$  as

$$L_m / L_i = F_0^{1/4} \nu^{-1/4} N^{-1/2} = Re^{1/4}, \quad (43)$$

and thus for  $Re > 1$  we obtain an ordering relation for the considered length scales:

$$L_i < L_m = L_i Re^{1/4} < L_e = L_i Re^{3/4}. \quad (44)$$

Similar considerations allow one to interpret  $L_e = V_e^2 / B_e$ , expressed in terms of momentum and buoyancy flux e-scales  $V_e^2$  and  $V_e B_e$ , as an analog of the Monin-Obukhov length scale [14]. On the other hand, within the framework of the proposed scaling hypothesis,  $L_e$  may also be treated as a characteristic length scale of turbulence in the e-region.

We propose further that the characteristic turbulence length scale  $L_c$  in the considered flow type changes linearly with distance from the wall within the range  $L_i \leq x \leq L_e$ , so that the characteristic turbulence wavenumber in this range is  $k_c = 2\pi / L_c \sim x^{-1}$ : with  $x \rightarrow L_i$ ,  $L_c \rightarrow L_i$ , and with  $x \rightarrow L_e$ ,  $L_c \rightarrow L_e$ .

In terms of  $Re = F_0 / (\nu N^2)$ , the e-scaled momentum and buoyancy equations and corresponding boundary conditions, (38)-(40), acquire the following forms:

$$b_e + \frac{1}{Re} \frac{\partial^2 w_e}{\partial x_e^2} - \frac{\partial \tau_e}{\partial x_e} = 0, \quad (45)$$

$$-w_e + \frac{1}{Re} \frac{\partial^2 b_e}{\partial x_e^2} - \frac{\partial F_e}{\partial x_e} = 0, \quad (46)$$

with boundary conditions:

$$w_{e0} = 0, \quad (db_e / dx_e)|_0 = -Re, \quad w_{e\infty} = 0, \quad b_{e\infty} = 0. \quad (47)$$

In accordance with the adopted scaling hypotheses, the mean velocity and buoyancy gradients in the i- and e-regions may be expressed in terms of corresponding governing scales as

$$\frac{\partial u}{\partial x} = f_{wi}(x, V_i, B_i), \quad \frac{\partial b}{\partial x} = f_{bi}(x, V_i, B_i), \quad (48)$$

and

$$\frac{\partial w}{\partial x} = f_{we}(x, V_e, B_e), \quad \frac{\partial b}{\partial x} = f_{be}(x, V_e, B_e), \quad (49)$$

respectively, or equivalently, using the  $\Pi$  theorem, as

$$\frac{L_i}{V_i} \frac{\partial w}{\partial x} \equiv \frac{\partial w_i}{\partial x_i} = \varphi_{wi}(x / L_i) \equiv \varphi_{wi}(x_i), \quad \frac{L_i}{B_i} \frac{\partial b}{\partial x} \equiv \frac{\partial b_i}{\partial x_i} = \varphi_{bi}(x / L_i) \equiv \varphi_{bi}(x_i), \quad (50)$$

$$\frac{L_e}{V_e} \frac{\partial w}{\partial x} \equiv \frac{\partial w_e}{\partial x_e} = \varphi_{we}(x/L_e) \equiv \varphi_{we}(x_e), \quad \frac{L_e}{B_e} \frac{\partial b}{\partial x} \equiv \frac{\partial b_e}{\partial x_e} = \varphi_{be}(x/L_e) \equiv \varphi_{be}(x_e), \quad (51)$$

where  $\varphi_{wi}$ ,  $\varphi_{bi}$ , and  $\varphi_{we}$ ,  $\varphi_{be}$  are dimensionless universal functions of the normalized distances  $x_i = x/L_i$  and  $x_e = x/L_e$ , respectively.

Adopting the scale matching methodology for high-Re number wall flows described in [13], one may match the i- and e-scaling laws for  $x$  within the distance range  $L_i \ll x \ll L_e$  to evaluate the behavior of the velocity and buoyancy gradients  $\partial w/\partial x$  and  $\partial b/\partial x$  in this range. According to (42), the existence of such intermediate distance range is conditioned by sufficiently large Re. Matching gradients of  $w$  and  $b$  in the double limit of  $x_i \rightarrow \infty$  and  $x_e \rightarrow 0$  yields

$$(V_i/L_i)\varphi_{wi}(x_i) = (V_e/L_e)\varphi_{we}(x_e), \quad (B_i/L_i)\varphi_{bi}(x_i) = (B_e/L_e)\varphi_{be}(x_e). \quad (52)$$

It follows from (36) and (37) that the scale of the kinetic energy production/dissipation rate in the i-region,  $V_i^3/L_i$ , is equal to the corresponding scale in the e-region,  $V_e^3/L_e$ , with both being equal to the surface energy production rate  $F_0$ . Equations (36) and (37) also show that the i- and e-scales of the thermal (potential) energy production/dissipation rate,  $V_i B_i$  and  $V_e B_e$ , are equal to each other and to  $F_0$ . We thus have

$$V_i^3/L_i = V_e^3/L_e = V_i B_i = V_e B_e = F_0. \quad (53)$$

Assuming the scale continuity in the entire distance interval  $L_i \leq x \leq L_e$ , one may introduce intermediate (local)  $x$ -scales for velocity,  $V_x$ , and buoyancy,  $B_x$ , which are related to each other as  $V_x^3/x = V_x B_x = F_s$  and which match the i- and e-scales at the ends of the interval  $L_i \leq x \leq L_e$ . The expressions  $V_i^3/L_i = V_x^3/x = V_e^3/L_e$  and  $V_i B_i = B_x V_x = V_e B_e$  provide  $V_i/L_i = V_x x_i^{2/3}/x$ ,  $V_e/L_e = V_x x_e^{2/3}/x$ ,  $B_i/L_i = B_x x_i^{4/3}/x$ , and  $B_e/L_e = B_x x_e^{4/3}/x$ . Substitution of these i-x-e scale relationships in (52) results in

$$x_i^{2/3} \varphi_{wi}(x_i) = x_e^{2/3} \varphi_{we}(x_e), \quad (54)$$

$$x_i^{4/3} \varphi_{bi}(x_i) = x_e^{4/3} \varphi_{be}(x_e). \quad (55)$$

The left-hand sides of (54) and (55) depend only on  $x_i$ , while the right-hand sides depend exclusively on  $x_e$ . In order to satisfy the matching requirement as  $x_i \rightarrow \infty$  and  $x_e \rightarrow 0$ , the functions on the both sides must asymptotically tend to universal constant values, so that

$$x_i^{2/3} \varphi_{wi}(x_i) = x_e^{2/3} \varphi_{we}(x_e) = -\frac{1}{\kappa_w}, \quad (56)$$

$$x_i^{4/3} \varphi_{bi}(x_i) = x_e^{4/3} \varphi_{be}(x_e) = -\frac{1}{\kappa_b}, \quad (57)$$

where the matching universal constants are introduced as  $-1/\kappa_w$  and  $-1/\kappa_b$ , with  $\kappa_w$  being analogous to the von Kármán constant in the traditional wall-flow theory [13]. Therefore, in the limit of  $x_i \rightarrow \infty$  and  $x_e \rightarrow 0$ , that is, in the range of  $L_i \ll x \ll L_e$  with  $Re \rightarrow \infty$ , the dimensionless gradients of  $w$  and  $b$  have the following asymptotic representations:

$$\varphi_{wi}(x_i) = -\frac{1}{\kappa_w} x_i^{-2/3}, \quad \varphi_{we}(x_e) = -\frac{1}{\kappa_w} x_e^{-2/3}, \quad (58)$$

$$\varphi_{bi}(x_i) = -\frac{1}{\kappa_b} x_i^{-4/3}, \quad \varphi_{be}(x_e) = -\frac{1}{\kappa_b} x_e^{-4/3}. \quad (59)$$

Taking into account that at small  $x_e$  the e-functions in (56)-(57) allow the following representations:

$$-\kappa_w x_e^{2/3} \varphi_{we}(x_e) = 1, \quad -\kappa_b x_e^{4/3} \varphi_{be}(x_e) = 1, \quad (60)$$

one may expand  $-\kappa_w x_e^{2/3} \varphi_{we}(x_e)$  and  $-\kappa_b x_e^{4/3} \varphi_{be}(x_e)$  into power series of  $x_e = x/L_e$  in the vicinity of  $x_e = 0$ . Keeping only linear terms given the smallness of  $x_e$ , we obtain

$$-\kappa_w x_e^{2/3} \varphi_{we}(x_e) = 1 + \alpha_w x_e, \quad -\kappa_b x_e^{4/3} \varphi_{be}(x_e) = 1 + \alpha_b x_e, \quad (61)$$

or

$$\varphi_{we}(x_e) = -\frac{x_e^{-2/3}}{\kappa_w} (1 + \alpha_w x_e), \quad \varphi_{be}(x_e) = -\frac{x_e^{-4/3}}{\kappa_b} (1 + \alpha_b x_e), \quad (62)$$

where  $\alpha_w$  and  $\alpha_b$  are constants. Equations (62) are expected to be asymptotically valid in the range of distances  $Re^{-3/4} = L_i/L_e \ll x_e < 1$ . The integration of (62) over  $x_e$  yields the following e-scaled power-law profiles of velocity and buoyancy:

$$w_e(x_e) = C_w - 3 \frac{x_e^{1/3}}{\kappa_u} (1 + \alpha_w x_e / 4), \quad b_e(x_e) = C_b + 3 \frac{x_e^{-1/3}}{\kappa_b} (1 - \alpha_b x_e / 2), \quad (63)$$

where  $C_w$  and  $C_b$  are integration constants.

The e-scaled governing equations (45)-(46) indicate that in the  $Re^{-3/4} = L_i/L_e \ll x_e < 1$  region of high-Re flow, where  $w_e$  and  $b_e$  are given by the dimensionless expressions (63), the dimensionless derivatives of turbulent fluxes,  $\partial\tau_e/\partial x_e$  and  $\partial F_e/\partial x_e$ , should integrate to the following asymptotic profiles

$$\tau_e(x_e) = C_\tau + C_b x_e + \frac{9z_e^{2/3}}{2\kappa_b} (1 - \alpha_b x_e / 5), \quad (64)$$

$$F_e(x_e) = C_F - C_w x_e + \frac{9z_e^{4/3}}{4\kappa_w} (1 + \alpha_w x_e / 7), \quad (65)$$

where  $C_\tau$ ,  $C_F$  are two other integration constants.

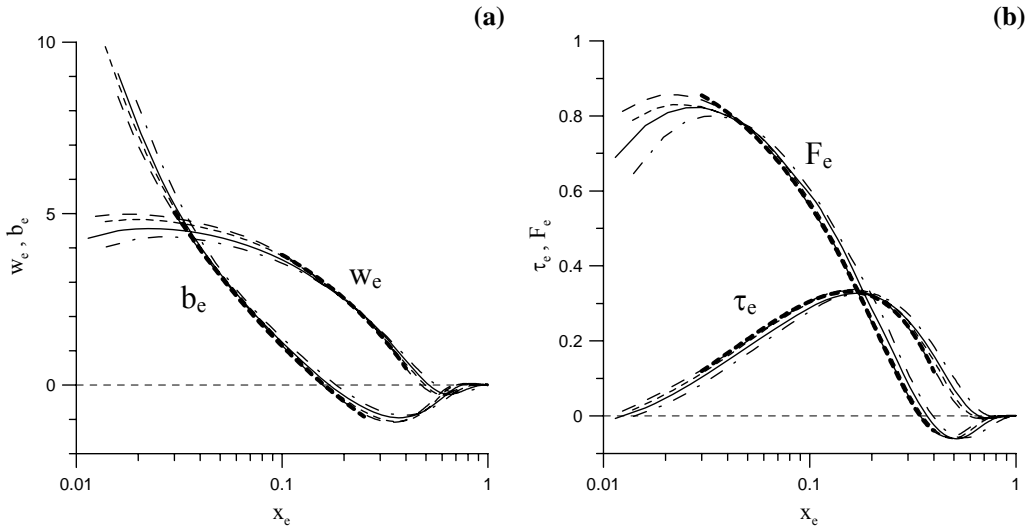


Fig. 8. E-scaled profiles of velocity and buoyancy (a) and momentum and buoyancy flux (b) profiles in numerically simulated turbulent convection flow for four different Re: 2000 (dashed and dotted lines), 3000 (solid lines), 4000 (short-dash lines), and 5000 (long-dash lines).

Predicted power-law approximations for  $w_e$  and  $b_e$ , Eqs. (63), and corresponding approximations for  $\tau_e$  and  $F_e$ , Eqs. (64) and (65), are indicated by bold dashed lines

The predicted features of  $w$ ,  $b$ ,  $\tau$ , and  $F$  profiles were verified against direct numerical simulation (DNS) data. The same numerical procedure as in [6] and [7] was employed. Flow cases with Re ranging from 2000 to 5000 were simulated. We then performed least-square fits of (63)-(65) to estimate the constants in these expressions fitting the highest-Re data. The results shown in Fig. 8 confirm that power-law expressions for the normalized velocity and buoyancy profiles, as well as the corresponding expressions for the profiles of fluxes, are indeed valid in the intermediate region.

## 5. SUMMARY

1. A set of problems related to the natural convection flow in a stratified fluid adjacent to a doubly infinite heated plate was studied analytically and numerically.
2. Analytical solutions were obtained for a laminar flow with a Prandtl number of unity for the cases of impulsive (step) change in plate perturbation temperature and for the sudden application of a plate heat flux. These flows were associated with a simple negative feedback mechanism: rising warm fluid cooled relative to the environment, whereas subsiding cool fluid warmed relative to the environment. Because of this feedback, the flow in stably stratified environment eventually approached a steady state, whereas the corresponding flow in a non-stratified fluid did not.
3. The dependence of convection of a stably stratified fluid along a vertical plate on the Prandtl number (Pr) was explored. The developing boundary layers were found to be

- thicker, more vigorous, and more sensitive to the Pr value at smaller Pr numbers ( $<1$ ) than at larger Pr numbers ( $>1$ ).
4. Analytical temperature and velocity solutions were obtained for a laminar natural convection flow resulting from temporally periodic variations in the plate surface temperature. The solutions indicated that this flow is composed of two waves that decay exponentially with distance from the surface: a fast long wave and a slow short wave. For forcing frequencies greater than the natural frequency of the corresponding inviscid system, these two waves propagate away from the surface. For forcing frequencies less than this natural frequency, the short wave propagates away from the surface while the long wave propagates toward the surface.
  5. Power-law intervals have been predicted in the mean velocity and buoyancy profiles of the developed statistically stationary turbulent natural convection flow of stratified fluid along a wall with a constant surface buoyancy (heat) flux. These predictions have been confirmed by direct numerical simulation of the considered convective flow at moderate Re numbers.

## REFERENCES

- [1] Prandtl L.: Führer durch die Strömungslehre, Vieweg und Sohn, Braunschweig, 1942.
- [2] Gebhart B., Jaluria Y., Mahajan R. L., Sammakia B.: Buoyancy-Induced Flows and Transport, Hemisphere, 1988.
- [3] Park J. S., Hyun J. M.: Transient behavior of vertical buoyancy layer in a stratified fluid, *Intl. J. Heat Mass Transfer*, Vol. 41 (1998), pp. 4393-4397.
- [4] Park J. S.: Transient buoyant flows of a stratified fluid in a vertical channel, *KSME Intl J.*, Vol. 15 (2001), pp. 656-664.
- [5] Shapiro A., Fedorovich E.: Unsteady convectively driven flow along a vertical plate immersed in a stably stratified fluid, *J. Fluid Mech.*, Vol. 498 (2004), pp. 333-352.
- [6] Shapiro A., Fedorovich E.: Prandtl-number dependence of unsteady natural convection along a vertical plate in a stably stratified fluid, *Int. J. Heat and Mass Transfer*, Vol. 47 (2004), pp. 4911-4927.
- [7] Shapiro A., Fedorovich E.: Natural convection in a stably stratified fluid along vertical plates and cylinders with temporally-periodic surface temperature variations, *J. Fluid Mech.*, Vol. 546 (2006), pp. 295-311.
- [8] Doetsch G.: Guide to the Applications of Laplace Transforms, Van Nostrand, 1961.
- [9] Goldstein R. J., Briggs, D. G.: Transient free convection about vertical Plates and circular cylinders, *Trans. ASME: J. Heat Transfer*, Vol. 86 (1964), pp. 490-500.
- [10] Fedorovich E., Nieuwstadt F. T. M., Kaiser R.: Numerical and laboratory study of horizontally evolving convective boundary layer. Part I: Transition regimes and development of the mixed layer, *J. Atmos. Sci.*, Vol. 58 (2001), pp. 70-86.
- [11] Pope S. B.: *Turbulent Flows*, Cambridge University Press, 2000.
- [12] Garratt J. R.: *The Atmospheric Boundary Layer*, Cambridge University Press, 1992.
- [13] Tennekes, H., Lumley J. L.: *A First Course in Turbulence*, The MIT Press, 1972.
- [14] Monin, A. S., Obukhov, A. M.: Basic laws of turbulent mixing in the atmosphere near the ground, *Tr. Akad. Nauk SSSR Geofiz. Inst.*, Vol. 24 (1954), pp. 163-187.